Al-Azhar Bulletin of Science

Volume 34 | Issue 2 Article 9

2023
Section: Mathematics and Statistics

A numerical study for covid-19 spatio-temporal lockdown model

Ahmed F. Koura
Basic Science Department, Al-Safwa High Institute of Engineering, Egypt.

Kamal R. Raslan
Mathematics Department, Faculty of Science, Al-Azhar University, Nasr-City, Cairo, Egypt

Khalid K. Ali
Mathematics Department, Faculty of Science, Al-Azhar University, Nasr-City, Cairo, Egypt

Mohamed A. Shaalan
Basic Science Department, Higher Technological Institute, 10thof Ramadan City, Egypt,
abozeid87@yahoo.com

How to Cite This Article

Koura, Ahmed F.; Raslan, Kamal R.; Ali, Khalid K.; and Shaalan, Mohamed A. (2023) "A numerical study for covid-19 spatio-temporal lockdown model," *Al-Azhar Bulletin of Science*: Vol. 34: Iss. 2, Article 9.
DOI: https://doi.org/10.58675/2636-3305.1651

ORIGINAL ARTICLE

A Numerical Study for Coronavirus Disease 2019 Spatio-temporal Lockdown Model

Ahmed Fikry Koura [a], Kamal Raslan Raslan [b], Khalid Karam Ali [b], Mohamed Abozeid Shaalan [c,*]

[a] Basic Science Department, Al-Safwa High Institute of Engineering, Egypt
[b] Mathematics Department, Faculty of Science, Al-Azhar University, Nasr-City, Cairo, Egypt
[c] Basic Science Department, Higher Technological Institute, 10th of Ramadan City, Egypt

Abstract

This article presents a detailed numerical study of lockdown (temporal and spatio-temporal) mathematical models for coronavirus disease 2019 (COVID-19). The temporal model proposed in this study comprises a system of five nonlinear ordinary differential equations, while the spatio-temporal model consists of five nonlinear partial differential equations. The reproduction number is discussed as a means to estimate the spread of the COVID-19 pandemic, and sensitivity analysis is performed to highlight the significance of pandemic parameters. Furthermore, the stability regions of the given models, as well as the Von Neumann stability and consistency of the numerical scheme applied to the spatio-temporal model, are investigated. To analyze the numerical results of the presented models under various parameters and facilitate comparison, effective methods such as the central finite difference (CFD) and Runge-Kutta of fifth order (RK-5) are applied. This comprehensive study provides insights into the dynamics and behavior of the COVID-19 pandemic under different scenarios, shedding light on the effectiveness of lockdown measures and the impact of various parameters on the spread of the disease.

Keywords: Central finite difference method, Reproduction number, Runge-Kutta of fifth method, Sensitivity analysis, Von Neumann stability

1. Introduction

All over the world, there are a great number of viruses, including coronavirus disease 2019 (COVID-19), which has infected millions of people and affected their health and the economy as well. Many natural phenomena and life problems are crystallized in the form of mathematical models that are dealt with analytically or numerically [1–4]. The transmission dynamics of the virus can be formulated in mathematical models that understand us and predict the dynamics of the virus [5–9]. In [10] Kucharski et al. combined datasets from inside and outside Wuhan and formulated it as a mathematical model to estimate the early dynamics of transmission of the infection and take control measures against the spread of the virus. Baba et al. applied some schemes such as ODE45, Euler, Runge-Kutta of second-order (RK-2), and RK-4 to a mathematical model of COVID-19 that represents the imposition of lockdown in Nigeria [11]. In Brazil, Valle [12] used an iterative method in the COVID-19 model that can estimate the total number of infections and deaths, and the observed data are in agreement with the results obtained by the Gompertz model. Mandal et al. [13] found that to control COVID-19 in India by reducing the contact of exposed and susceptible humans to avoid imposing control measures by the government, In [14] Biswas et al. studied a model of the spreading of COVID-19, they estimated the parameters of the model by fitting the model with collected data about the virus in India and presented predictions with the future trends of COVID-19 transmission under some control measures. Zhang et al. [15] applied RK-4 to evaluate and analyze a new fractional-order mathematical model for the COVID-19 pandemic. Agarwal et al. analyzed the COVID-19 mathematical model of fractional order theoretically [16]. In [17] Wrapp et al. showed that the infected people who show symptoms are more numerous than those who do not show symptoms. Rothe et al. [18]

Received 19 July 2023; revised 21 August 2023; accepted 28 August 2023.
Available online 18 October 2023

* Corresponding author at: Higher Technological Institute, Egypt.
E-mail address: abozeid87@yahoo.com (M.A. Shaalan).

https://doi.org/10.58675/2636-3305.1651

discovered that the COVID-19 virus has more links than the severe acute respiratory syndrome (SARS) virus. In [19] Hakimeh et al. introduced a mathematical model to reduce the transmission of some diseases by the Caputo fractionalorder derivative. A numerical simulation was presented by Tuan et al. in [20] which obtained the approximate solutions by using the generalized Adams-Bashforth-Moulton method.

This article is arranged as follows: In section 2, we present a mathematical formulation for the COVID-19 lockdown (temporal and spatio-temporal) models. We investigate reproduction number, sensitivity analysis, and stability region analysis for the presented model, as shown in section 3. In section 4, we introduce numerical solutions for the COVID-19 temporal model via two schemes: RK-5 order and the central finite difference. In section 5, we introduce numerical solutions for the COVID-19 spatio-temporal model, study the stability and consistency of the numerical scheme, and discuss the results of the proposed model. In section 6, we discuss the effect of some parameters on controlling the spread of infection between individuals.

2. Mathematical formulation

In this section, we introduce a mathematical model of COVID-19 that describes the effect of lockdown strategies on the spread of COVID-19 between people. The population is divided into five categories: $S(t)$ represents the susceptible people that are not under lockdown; $S_Q(t)$ represents susceptible persons that are already under lockdown; $I(t)$ represents infected people who are not under lockdown; $I_Q(t)$ represents infected persons who are under lockdown at the same time; and $Q(t)$ is the cumulative density of the lockdown program. This model can be covered by a system of five nonlinear ordinary differential equations as a temporal model and a system of five nonlinear partial differential equations as a spatio-temporal model.

2.1. Temporal model

$$\begin{aligned}
\frac{dS}{dt} &= \Lambda - \beta SI - \delta_s SQ - dS + \mu_i I + \mu_q I_Q + \nu_s S_Q,\\
\frac{dS_Q}{dt} &= \delta_s SQ - dS_Q - \nu_s S_Q,\\
\frac{dI}{dt} &= \beta SI - \mu_i I - \rho_i I - dI - \delta_i IQ - \nu_i I_Q,\\
\frac{dI_Q}{dt} &= \delta_i IQ - dI_Q - \mu_q I_Q - \rho_q I_Q,\\
\frac{dQ}{dt} &= \eta I - \psi Q\,.
\end{aligned} \tag{2.1}$$

Subject to non-negative initial conditions:

$$S(0)=S_0, S_Q(0)=S_{Q0}, I(0)=I_0, I_Q(0)=I_{Q0}, Q(0)=Q_0\,. \tag{2.2}$$

2.2. Spatio-temporal model

$$\begin{aligned}
\frac{\partial S}{\partial t} &= C_1\frac{\partial^2 S}{\partial x^2} + \Lambda - \beta SI - \delta_s SQ - dS + \mu_i I + \mu_q I_Q + \nu_s S_Q,\\
\frac{\partial S_Q}{\partial t} &= C_2\frac{\partial^2 S_Q}{\partial x^2} + \delta_s SQ - dS_Q - \nu_s S_Q,\\
\frac{\partial I}{\partial t} &= C_3\frac{\partial^2 I}{\partial x^2} + \beta SI - \mu_i I - \rho_i I - dI - \delta_i IQ - \nu_i I_Q,\\
\frac{\partial I_Q}{\partial t} &= C_4\frac{\partial^2 I_Q}{\partial x^2} + \delta_i IQ - dI_Q - \mu_q I_Q - \rho_q I_Q,\\
\frac{\partial Q}{\partial t} &= C_5\frac{\partial^2 Q}{\partial x^2} + \eta I - \psi Q\,.
\end{aligned} \tag{2.3}$$

With initial conditions,

$$\begin{aligned}
S(0,x) &= \begin{cases} 2S_0 x & 0\le x\le 0.5\\ 2S_0(1-x) & 0.5\le x\le 1\end{cases},\\
S_Q(0,x) &= \begin{cases} 2S_{Q0} x & 0\le x\le 0.5\\ 2S_{Q0}(1-x) & 0.5\le x\le 1\end{cases},\\
I(0,x) &= \begin{cases} 2I_0 x & 0\le x\le 0.5\\ 2I_0(1-x) & 0.5\le x\le 1\end{cases},\\
I_Q(0,x) &= \begin{cases} 2I_{Q0} x & 0\le x\le 0.5\\ 2I_{Q0}(1-x) & 0.5\le x\le 1\end{cases},\\
Q(0,x) &= \begin{cases} 2Q_0 x & 0\le x\le 0.5\\ 2Q_0(1-x) & 0.5\le x\le 1\end{cases}.
\end{aligned} \tag{2.4}$$

And homogeneous Neumann boundary conditions,

$$\begin{aligned}
\frac{\partial S(t,0)}{\partial x} &= \frac{\partial S(t,1)}{\partial x} = 0,\\
\frac{\partial S_Q(t,0)}{\partial x} &= \frac{\partial S_Q(t,1)}{\partial x} = 0,\\
\frac{\partial I(t,0)}{\partial x} &= \frac{\partial I(t,1)}{\partial x} = 0,\\
\frac{\partial I_Q(t,0)}{\partial x} &= \frac{\partial I_Q(t,1)}{\partial x} = 0,\\
\frac{\partial Q(t,0)}{\partial x} &= \frac{\partial Q(t,1)}{\partial x} = 0.
\end{aligned} \tag{2.5}$$

Where Λ is the rate of recruitment, β rate of infection contact, δ_s and δ_i lockdown imposition on susceptible and infected persons respectively, ρ_i and ρ_q rate of death in infected persons but not under lockdown and infected persons under lockdown respectively, μ_i and μ_q rate of recovery in infected persons but not under lockdown and infected persons under lockdown, ν_s transfer rate of susceptible lockdown persons to susceptible class, ν_i transfer rate of infection of persons under lockdown to infection class, η achievement rate of the lockdown program and ψ depletion rate of the lockdown program.

3. Reproduction number and stability region

In this section, we introduce some important indicators that help us realize the spread of the pandemic in the population.

3.1. Reproduction number

The number of new infections caused by an infectious individual in a disease-free population is defined as the reproduction number R_0. If $R_0 > 1$, the pandemic will spread, while it will be confined if $R_0 < 1$ To obtain R_0 for the proposed model (2.1) we put the virus-free equilibrium point $C_0 = [S_0, 0, 0, 0, 0]$ and make the system (2.1) equal to zero and solve it.

$$\begin{aligned}
0 &= \Lambda - \beta SI - \delta_s SQ - dS + \mu_i I + \mu_q I_Q + \nu_s S_Q,\\
0 &= \delta_s SQ - dS_Q - \nu_s S_Q,\\
0 &= \beta SI - \mu_i I - \rho_i I - dI - \delta_i IQ + \nu_i I_Q,\\
0 &= \delta_i IQ - dI_Q - \nu_i I_Q - \mu_q I_Q - \rho_q I_Q,\\
0 &= \eta I - \psi Q.
\end{aligned} \tag{3.1}$$

We get $S_0 = \frac{\Lambda}{d}$.

Let $X = [I, I_Q]^T$ which I and I_Q are components of the infection in the model and

$$\frac{dX}{dt} = F(X) - V(X), \tag{3.2}$$

Where

$$F(X) = \begin{pmatrix} \beta SI - \delta_i IQ \\ \delta_i IQ \end{pmatrix}, V(X) = \begin{pmatrix} \mu_i I + \rho_i I + dI - \nu_i I_Q \\ dI_Q + \nu_i I_Q + \mu_q I_Q + \rho_q I_Q \end{pmatrix}.$$

$$J(F(X)) = \begin{pmatrix} \beta S - \delta_i Q & 0 \\ \delta_i Q & 0 \end{pmatrix}, J(V(X)) = \begin{pmatrix} \mu_i + \rho_i + d & -\nu_i \\ 0 & d + \nu_i + \mu_q + \rho_q \end{pmatrix}, \tag{3.3}$$

where $J(F(X))$ and $J(V(X))$ are the Jacobians of $F(X)$ and $V(X)$ respectively.

We calculate the greatest eigenvalue of the matrix $J(F(X)) * J(V(X))^{-1}$ and substitute with C_0, we obtain the reproduction number R_0 for the model (2.1).

$$R_0 = \frac{\beta\Lambda}{d\rho_i + d^2 + d\mu_i}. \tag{3.4}$$

3.2. Sensitivity analysis

The sensitivity analysis is studying the pandemic parameters of the proposed model (2.1) and their effects on the virus spread. Using the reproduction number R_0 we obtain

$$\begin{aligned}
\frac{\partial R_0}{\partial \Lambda} &= \frac{\beta}{d\rho_i + d^2 + d\mu_i},\\
\frac{\partial R_0}{\partial \beta} &= \frac{\Lambda}{d\rho_i + d^2 + d\mu_i},\\
\frac{\partial R_0}{\partial d} &= \frac{-\beta\Lambda(\rho_i + 2d + \mu_i)}{(d\rho_i + d^2 + d\mu_i)^2},\\
\frac{\partial R_0}{\partial \rho_i} &= \frac{-\beta\Lambda}{(d\rho_i + d^2 + d\mu_i)^2},\\
\frac{\partial R_0}{\partial \mu_i} &= \frac{-\beta\Lambda d}{(d\rho_i + d^2 + d\mu_i)^2}.
\end{aligned} \tag{3.5}$$

Given that all parameters are positive, then we have $\frac{\partial R_0}{\partial \Lambda} > 0, \frac{\partial R_0}{\partial \beta} > 0$ and $\frac{\partial R_0}{\partial d} < 0, \frac{\partial R_0}{\partial \rho_i} < 0, \frac{\partial R_0}{\partial \mu_i} < 0$.

Thus, increasing the parameters Λ and β results in an increase in R_0, and increasing the parameters d, ρ_i, and μ_i leads to a decrease in R_0.

3.3. Stability region

In the region of stability of the disease-free equilibrium and endemic points shown for (ρ_i, μ_i, β) in Figs. 1 and 2 the values of other parameters are fixed. In Fig. 1, we examine the effects of (ρ_i, μ_i, β) at the disease-free equilibrium point where $R_0 < 1$. Fig. 1b, c, d illustrates the projection of the stability region (ρ_i, β) with fixed μ_i at 0.15, 0.25, and 0.45, respectively. We observe that ρ_i and β maintain their stability at a large value of μ_i.

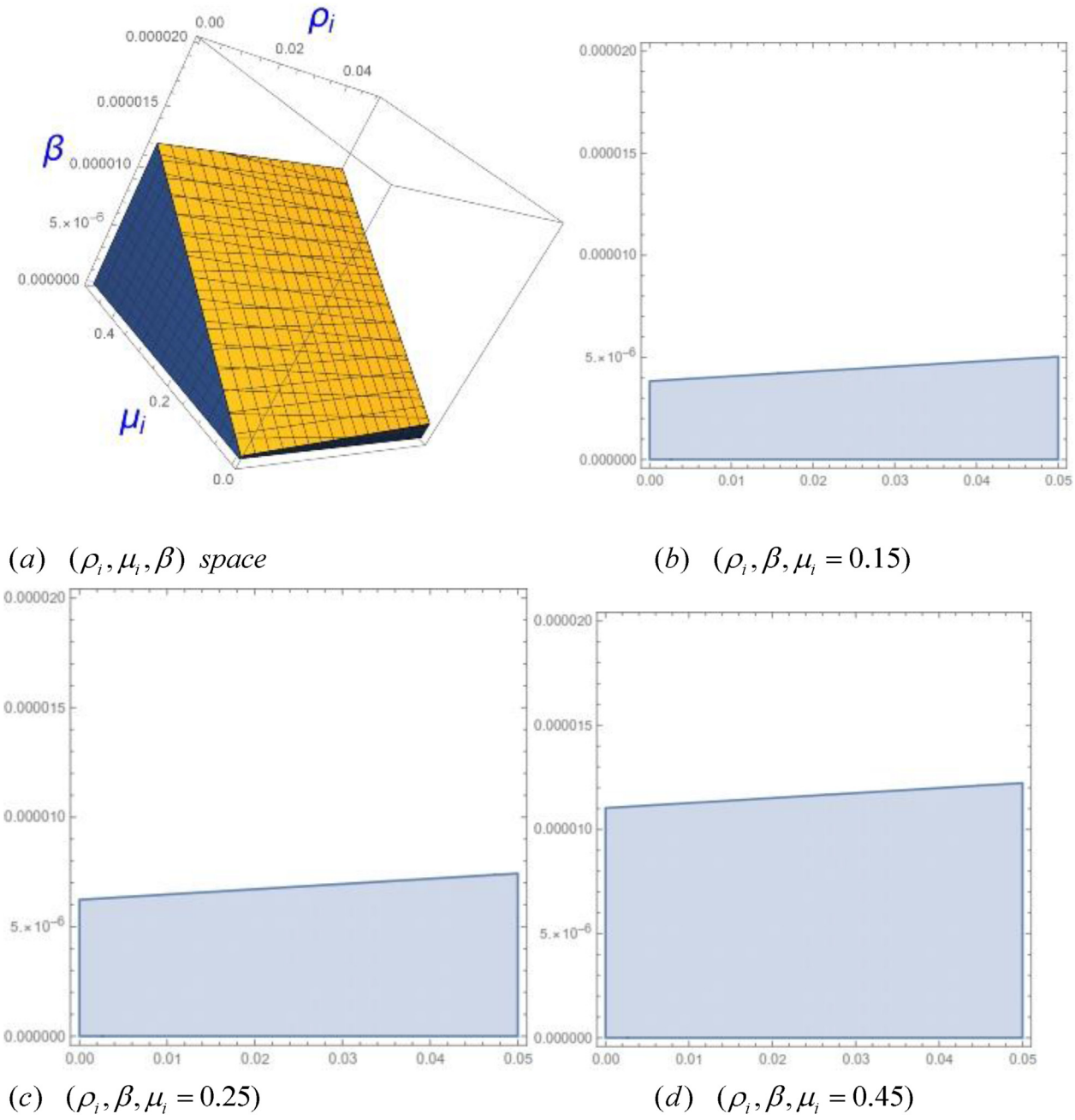

Fig. 1. Stability region for disease free equilibrium point.

In Fig. 2, we examine the effects of (ρ_i, μ_i, β) at the endemic equilibrium point. Figure 2b, c, d illustrates the projection of the stability region (ρ_i, β) with fixed μ_i at 0.15, 0.25, and 0.45, respectively. We observe that ρ_i and β maintain their stability at a small value of μ_i.

4. Numerical solutions for temporal model

This section presents the computational methods of the endemic model of COVID-19 2.1. We took some parameter values from the works of literature and estimated the other parameter values from the stability region, which is discussed in Section 3. We carry out two efficient numerical schemes: RK-5-order and central finite-difference.

The RK-5 method provides a higher degree of stability, making it effective in handling stiff ODEs where the solution changes rapidly. Stiff ODEs often require smaller step sizes to maintain accuracy, but the RK-5 method can still provide accurate results even with relatively larger step sizes compared with

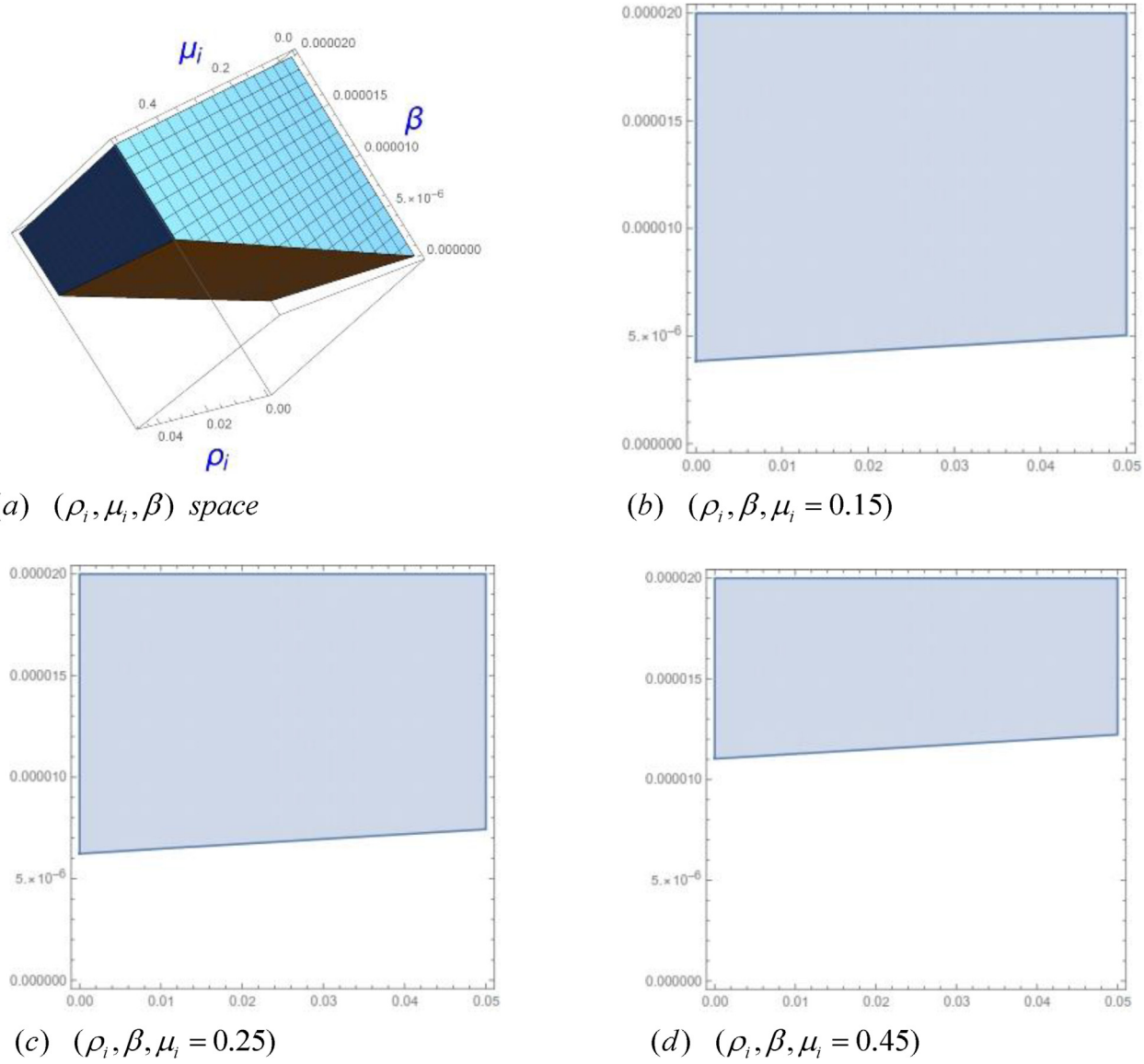

Fig. 2. Stability region for endemic equilibrium point.

lower-order methods. The main objectives in choosing a higher order central finite difference method are accuracy and stability. Higher order methods approximate derivatives using more points, leading to smaller errors. They are also often more numerically stable, allowing a larger time step size. This improves computational efficiency by enabling the use of a coarser grid for a given accuracy. Higher order central finite difference methods generally provide a better balance of accuracy, stability and efficiency compared with lower order methods for solving ODEs.

4.1. Runge-Kutta 5th order (RK-5)

Assume that the initial value problem is well-posed, then

$$\frac{dy}{dt} = F(t,y), a < t < b, y(a) = e, \tag{4.1}$$

we establish the RK-5 technique by a sequence of approximation points $(t, w_i) \simeq (t, y(t))$ to the exact solution of Equation (4.1) by

$$t_{i+1} = t_i + h,$$
$$k_1 = F(t_i, w_i),$$
$$k_2 = F\left(t_i + \frac{h}{4}, w_i + \frac{k_1 h}{4}\right),$$
$$k_3 = F\left(t_i + \frac{h}{4}, w_i + \frac{k_1 h}{8} + \frac{k_2 h}{8}\right),$$
$$k_4 = F\left(t_i + \frac{h}{2}, w_i - \frac{k_2 h}{2} + k_3 h\right),$$
$$k_5 = F\left(t_i + \frac{3h}{4}, w_i + \frac{3k_1 h}{16} + \frac{9k_4 h}{16}\right),$$
$$k_6 = F\left(t_i + h, w_i - \frac{3k_1 h}{7} + \frac{2k_2 h}{7} + \frac{12k_3 h}{7} - \frac{12k_4 h}{7} + \frac{8k_5 h}{7}\right),$$
$$w_{i+1} = w_i + \frac{h}{90}(7k_1 + 32k_3 + 12k_4 + 32k_5 + 7k_6).$$

4.2. Central finite difference (CDF)

Suppose that a well-posed IVP (4.1) is given the central finite difference (CFD) technique as a sequence of approximation points $(t_i, w_i) \simeq (t_i, y(t_i))$ to the exact solution of Equation (4.1) by

$$t_{i+1} = t_i + k,$$
$$\frac{dy}{dt} = \frac{F(t_i, w_i + k) + F(t_i, w_i - k)}{2k}.$$

4.3. Results

Now, we discuss the numerical outcomes of the governing model with respect to the approximate solutions. To achieve this aim, we employed the effective Central Finite Difference and RK-5 schemes and compared the results after 200 days. The initial conditions as discussed in [11] are $S(0) = 400, S_Q(0) = 300, I(0) = 300, I_Q(0) = 497$, and $Q(0) = 200$, and the parameter values are $\Lambda = 400, \delta_s = 0.0002, \nu_s = 0.2, \eta = 0.0005, \psi = 0.06$, $\mu_i = \mu_q = 0.16979, \rho_q = 0.03275$, $\delta_i = 0.002, \nu_i = 0.02$, $d = 0.0096$, and assuming the values of $\beta = 0.000017$, $\rho_i = 0.03275$. Using the Mathematica package, we apply our techniques of CFD and RK-5 to solve the proposed model 2.1.

Figs. 3–7 represent the solution of the system (2.1). It can be demonstrated that the RK-5 method gives a better approximation than the CFD method.

All figures show that the results of the model converge to their equilibrium points.

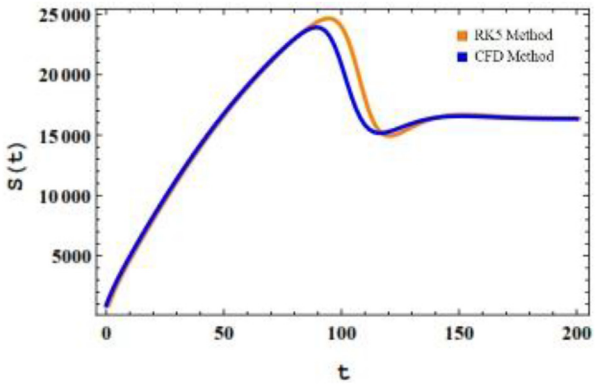

Fig. 3. Runge-Kutta of fifth order versus central finite difference for $S(t)$.

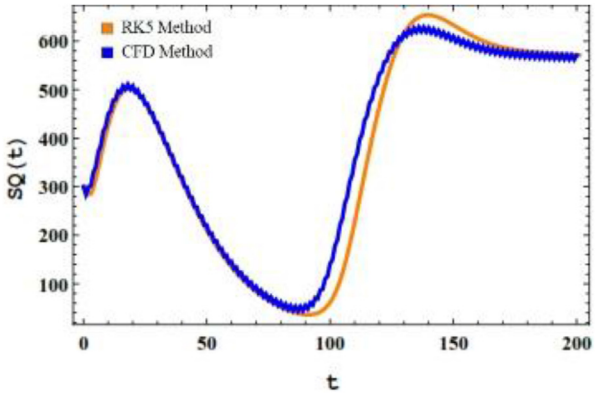

Fig. 4. Runge-Kutta of fifth order versus central finite difference for $S_Q(t)$.

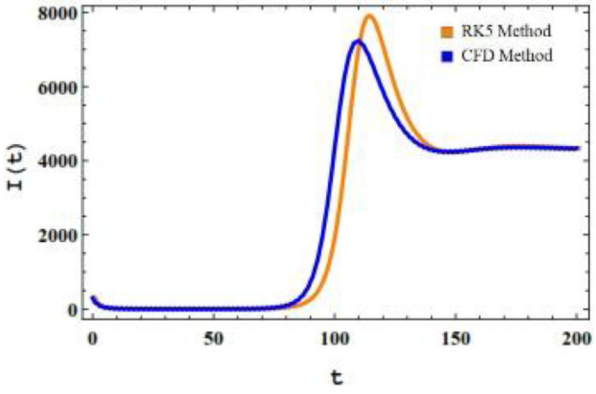

Fig. 5. Runge-Kutta of fifth order versus central finite difference for $I(t)$.

In Figs. 8–12, we introduce solutions with different values of $\delta_i = 0.002$, 0.001, and 0.003 that represent the imposition of lockdown on infected individuals to support the validity of our results.

Finally, from all the figures, we can confirm the effectiveness of the proposed algorithms and their computationally appropriate use of numerical handling of the given model.

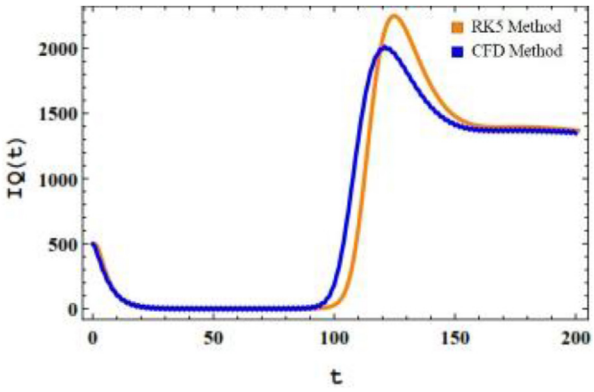

Fig. 6. Runge-Kutta of fifth order versus central finite difference for $I_Q(t)$.

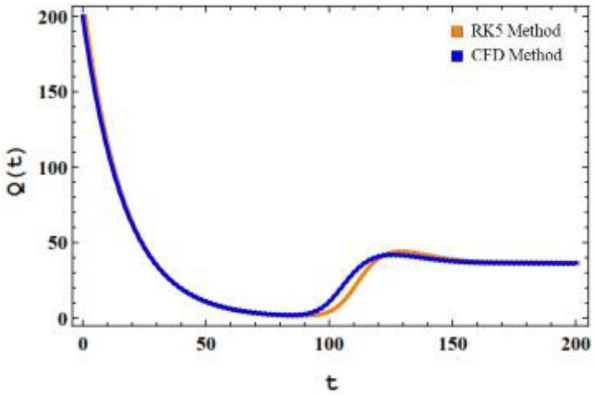

Fig. 7. Runge-Kutta of fifth order versus central finite difference for $Q(t)$.

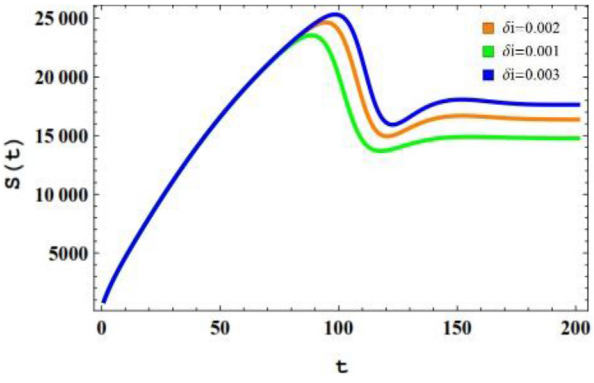

Fig. 8. Compare between different values of δ_i for $S(t)$.

5. Numerical solution for spatio-temporal model

In this section, we present a numerical simulation of the spatiotemporal model 2.3 with initial conditions 2.4 and boundary conditions 2.5 beginning with dividing the domain of x ∈ [0,1] and $t \in [0,200]$ into $10^2 \times 200$ cubes with step size $h = 0.1$ and $\tau = 1$.

For this, we apply finite difference using

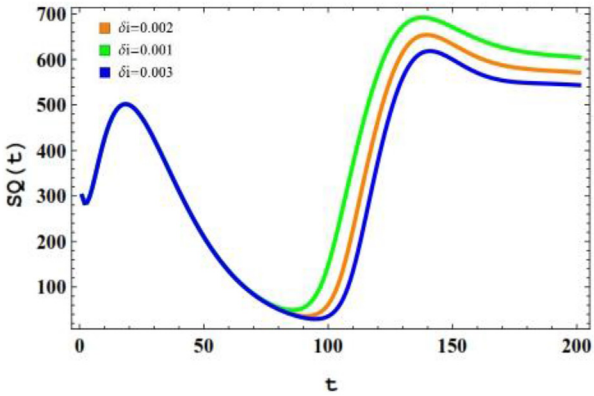

Fig. 9. Compare between different values of δ_i for $S_Q(t)$.

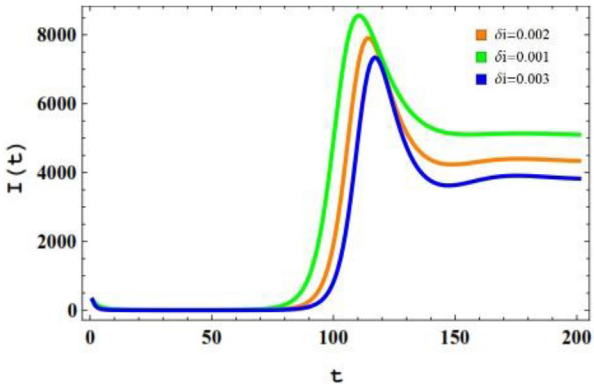

Fig. 10. Compare between different values of δ_i for $I(t)$.

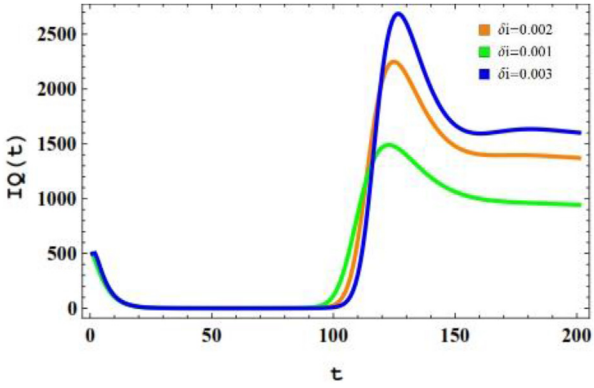

Fig. 11. Compare between different values of δ_i for $I_Q(t)$.

$$\frac{\partial f(t,x)}{\partial t} = \frac{f_i^{n+1} - f_i^n}{\tau},$$
$$\frac{\partial^2 f(t,x)}{\partial x^2} = \frac{f_{i-1}^{n+1} - 2f_i^{n+1} + f_{i+1}^{n+1}}{h^2}, \quad (5.1)$$
$$\frac{\partial f(t,x)}{\partial x} = \frac{f_{i+1}^n - f_{i-1}^n}{2h},$$

and then discretizing the system and its boundary conditions we get the following results,

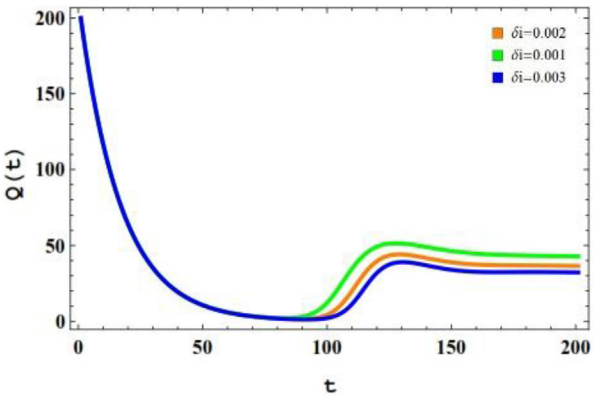

Fig. 12. Compare between different values of δ_i for $Q(t)$.

$$(S)_i^{n+1} = (S)_i^n + \frac{\tau C_1}{h^2}\left((S)_{i+1}^{n+1} - 2(S)_i^{n+1} + (S)_{i-1}^{n+1}\right) + \Lambda - \beta(S)_i^{n+1}(I)_i^n - \delta_s(S)_i^{n+1}(Q)_i^n - d(S)_i^{n+1} + \mu_i(I)_i^n + \mu_q(I_Q)_i^n + v_s(S_Q)_i^{n+1}, \tag{5.2}$$

$$(S_Q)_i^{n+1} = (S_Q)_i^n + \frac{\tau C_1}{h^2}\left((S_Q)_{i+1}^{n+1} - 2(S_Q)_i^{n+1} + (S_Q)_{i-1}^{n+1}\right) + I_i^{n+1}\delta_s(S)_i^n(Q)_i^n - d(S_Q)_i^{n+1} - v_s(S_Q)_i^{n+1}, \tag{5.3}$$

$$I_i^{n+1} = I_i^n + \frac{\tau C_3}{h^2}(I_{i+1}^{n+1} - 2I_i^{n+1} + I_{i-1}^{n+1}) + \beta(S)_i^n I_i^{n+1} - \mu_i I_i^{n+1} - \rho_i I_i^{n+1} - dI_i^{n+1} - \delta_i I(Q)_i^n + \nu_i(I_Q)_i^n, \tag{5.4}$$

$$(I_Q)_i^{n+1} = (I_Q)_i^n + \frac{\tau C_1}{h^2}\left((I_Q)_{i+1}^{n+1} - 2(I_Q)_i^{n+1} + (I_Q)_{i-1}^{n+1}\right) + \delta_i I_l^n Q_i^n - d(I_Q)_i^{n+1} - v_i(I_Q)_i^{n+1} - \mu_q(I_Q)_i^{n+1} - \rho_q(I_Q)_i^{n+1}, \tag{5.5}$$

$$Q_i^{n+1} = Q_i{}^n + \frac{\tau C_3}{h^2}(Q_{i+1}^{n+1} - 2Q_i^{n+1} + Q_{i-1}^{n+1}) + \eta I_i{}^n - \psi Q_i^{n+1}. \tag{5.6}$$

5.1. Stability of numerical scheme

In this subsection, we will test Von Neumann stability for the numerical method that we have applied.

Assume

$$\begin{aligned} S_i^n &= \xi_1^n e^{Jk_s ih}, \\ S_i^{n+1} &= \xi_1^{n+1} e^{Jk_s ih}, \\ S_{i+1}^n &= \xi_1^n e^{Jk_s(i+1)h}, \\ S_{i-1}^n &= \xi_1^n e^{Jk_s(i-1)h}, \end{aligned} \tag{5.7}$$

substitute from (5.7) in equation (5.2) we get the following relation,

$$\begin{aligned} \xi_1^{n+1}e^{Jk_s ih} = \xi_1^n e^{Jk_s ih} + \frac{\tau C_1}{h^2}\left(\xi_1^{n+1}e^{Jk_s(i+1)h} - 2\xi_1^{n+1}e^{Jk_s ih}\right. \\ \left. + \xi_1^{n+1}e^{Jk_s(i-1)h}\right) + \Lambda - \beta\xi_1^{n+1}e^{Jk_s ih}(I)_i^n \\ - \delta_s\xi_1^{n+1}e^{Jk_s ih}(Q)_i^n - d\xi_1^{n+1}e^{Jk_s ih} \\ + \mu_i(I)_i^n + \mu_q(I_Q)_i^n + \nu_s(S_Q)_i^n. \end{aligned} \tag{5.8}$$

Define the amplification factor $G_1 = \frac{S_i^{n+1}}{S_i^n}$, we can compute G_1 by dividing equation (5.8) by S_i^n and obtain

$$G_1 = 1 + \frac{\tau C_1}{h^2}\left(G_1 e^{Jk_S h} - 2G_1 + G_1 e^{-Jk_S h}\right) + \Lambda - \beta G_1(I)_i^n - \delta_s G_1(Q)_i^n - dG_1 + \mu_i(I)_i^n + \mu_q(I_Q)_i^n + \nu_s(S_Q)_i^n,$$

$$G_1 = \frac{1}{1 + 4\frac{\tau C_1}{h^2}sin^2\left(\frac{k_{S_a}h}{2}\right) + \tau\left(v_a^{\cdot} + d\right)},$$

$$G_1 = \left|\frac{1}{1 + 4\frac{\tau C_1}{h^2}sin^2\left(\frac{k_{S_a}h}{2}\right) + \tau\left(v_a^{\cdot} + d\right)}\right| \le 1. \tag{5.9}$$

Similarly, repeating the previous steps to equations (5.3)–(5.6) for $(S_Q)_i^n$, I_i^n, $(I_Q)_i^n$, and Q_i^n with $(S_Q)_i^n = \xi_2^n e^{Jk_{s_q} ih}$, $I_i^n = \xi_3^n e^{Jk_I ih}$, $(I_Q)_i^n = \xi_4^n e^{Jk_{(I_Q)} ih}$, and $Q_i^n = \xi_5^n e^{Jk_Q ih}$ respectively, we also obtain

$$G_2 = \left|\frac{1}{1 + 4\frac{\tau C_2}{h^2}sin^2\left(\frac{k_{S_b}h}{2}\right) + \tau(d + \nu_s)}\right| \le 1, \tag{5.10}$$

$$G_3 = \left|\frac{1}{1 + 4\frac{\tau C_3}{h^2}sin^2\left(\frac{k_I h}{2}\right) + \tau\left(\mu_i + \rho_i + d + v_b^{\cdot}\right)}\right| \le 1, \tag{5.11}$$

$$G_4 = \left|\frac{1}{1 + 4\frac{\tau C_4}{h^2}sin^2\left(\frac{k_{(I_Q)}h}{2}\right) + \tau\left(d + \nu_i + \mu_q + \rho_q\right)}\right| \le 1, \tag{5.12}$$

$$G_5 = \left| \frac{1}{1 + 4\frac{\tau C_5}{h^2} sin^2\left(\frac{k_Q h}{2}\right) + \tau\psi} \right| \leq 1. \tag{5.13}$$

Where $v_a^{\cdot} = \beta I_i^n + \delta_s Q_i^n, v_b^{\cdot} = \delta_i Q_i^n - \beta S_i^n$ and $J = \sqrt{-1}$.

So $G_i \leq 1, i = 1,2,3,4,5$ which is the necessary and sufficient condition for the error to remain bounded and maintain von Nemann stability for the numerical method.

5.2. Consistency

In this subsection, we will use Taylor expansion to prove that this numerical scheme is first-order consistent in t and second-order consistent in x. For this, we use

$$\begin{aligned}\Phi_S = &\frac{S_i^{n+1} - S_i^n}{\tau} - \frac{C_1}{h^2}\left(S_{i+1}^{n+1} - 2S_i^{n+1} + S_{j-1}^{n+1}\right) - \Lambda \\ &+ \beta(S)_i^{n+1}(I)_i^n + \delta_s(S)_i^{n+1}(Q)_i^n + d(S)_i^{n+1} - \mu_i(I)_i^n \\ &- \mu_q\left(I_Q\right)_i^n - \nu_s\left(S_Q\right)_i^{n+1},\end{aligned}$$

$$\begin{aligned}\Phi_S = &\left(\frac{\partial S}{\partial t} + \frac{\tau}{2!}\frac{\partial^2 S}{\partial t^2} + \frac{\tau^2}{3!}\frac{\partial^2 S}{\partial t^2} + \ldots\right) - \frac{C_1}{h^2}\left(h^2\left(\frac{\partial^2 S}{\partial x^2} + 2\frac{h^2}{4!}\frac{\partial^4 S}{\partial x^2} + \ldots\right)\right) \\ &-\Lambda + \beta(I)_i^n + \delta_s(Q)_i^n + d - \nu_s * \left(S_i^n + \tau\frac{\partial S}{\partial t} + \frac{\tau^2}{2!}\frac{\partial^2 S}{\partial t^2} + \frac{\tau^3}{3!}\frac{\partial^2 S}{\partial t^2} + \ldots\right),\end{aligned}$$

$$\Phi_S = -\frac{C_1 h^2}{12}\left(\frac{\partial^4 S}{\partial x^4}\right) + \tau\left(\left(\beta I_i^n + \delta_s Q_i^n + d\right)\frac{\partial S_a}{\partial t} + \ldots\right),$$

which devolve to zero as τ, h become zero.

Also, we can obtain the relations of $S_Q, I, I_Q,$ and Q using the previous steps as follows:

$$\Phi_{S_Q} = -\frac{C_2 h^2}{12}\left(\frac{\partial^4 S_Q}{\partial x^4}\right) + \tau\left(\alpha_b I_i^n + \delta\right)\left(\frac{\partial S_Q}{\partial t} + \ldots\right),$$

$$\Phi_I = -\frac{C_3 h^2}{12}\left(\frac{\partial^4 I}{\partial x^4}\right) + \tau(\mu_i + \rho_i + d + \delta_i Q_i^n - \beta S_i^n)\left(\frac{\partial I}{\partial t} + \ldots\right),$$

$$\Phi_{I_Q} = -\frac{C_4 h^2}{12}\left(\frac{\partial^4 I_Q}{\partial x^4}\right) + \tau\left(d + \nu_i + \mu_q + \rho_q\right)\left(\frac{\partial I_Q}{\partial t} + \ldots\right),$$

$$\Phi_Q = -\frac{C_5 h^2}{12}\left(\frac{\partial^4 Q}{\partial x^4}\right) + \tau(\psi)\left(\frac{\partial Q}{\partial t} + \ldots\right),$$

which also go to zero as τ, h become zero. For this reason, the order of accuracy of this numerical method is $h^2 + \tau$.

5.3. Results

By solve the system (5.2)–(5.6) with the values of parameters that were extracted and discussed in sections 3 and 4, taking the values $C_i = 0.01$ and $i = 1, 2, 3, 4, 5$.

The Neumann boundary condition states that in complete lockdown, nobody can leave or enter the region. We can see in Fig. 13 that the numerical solution at the endemic equilibrium state at the selected parameters has good agreement with the chosen parameters.

All classes attain their maximum value in a specific region x and then decrease when they go away from this area.

6. Effects of parameters

The value of each parameter in the model affects the spread of the disease. The most important issue in controlling epidemics is creating lockdown to reduce relationships between individuals. In these models (temporal and spatio-temporal), we studied the effect of some parameters on infection classes I and I_Q. In these models, β represents the rate of infectious contact, which in turn affects the increase or decrease in the number of infected people, as shown in Fig. 14. The lower the values of β decrease the infection rate, which indicates that the lack of contact between people leads to the disappearance of the epidemic or at least a decrease in cases of disease. On the other hand, as shown in Fig. 15, by reducing ν_i, which represents the transmission of people from I_Q to I class, the number of infections decreases with the passage of time, which shows the role of isolation in reducing the spread of the disease. We also note an increase in μ_q, which represents the percentage of people recovering from the disease and were under lockdown, significantly reducing the number of infected people and under lockdown, as shown in Fig. 16b and d, but the

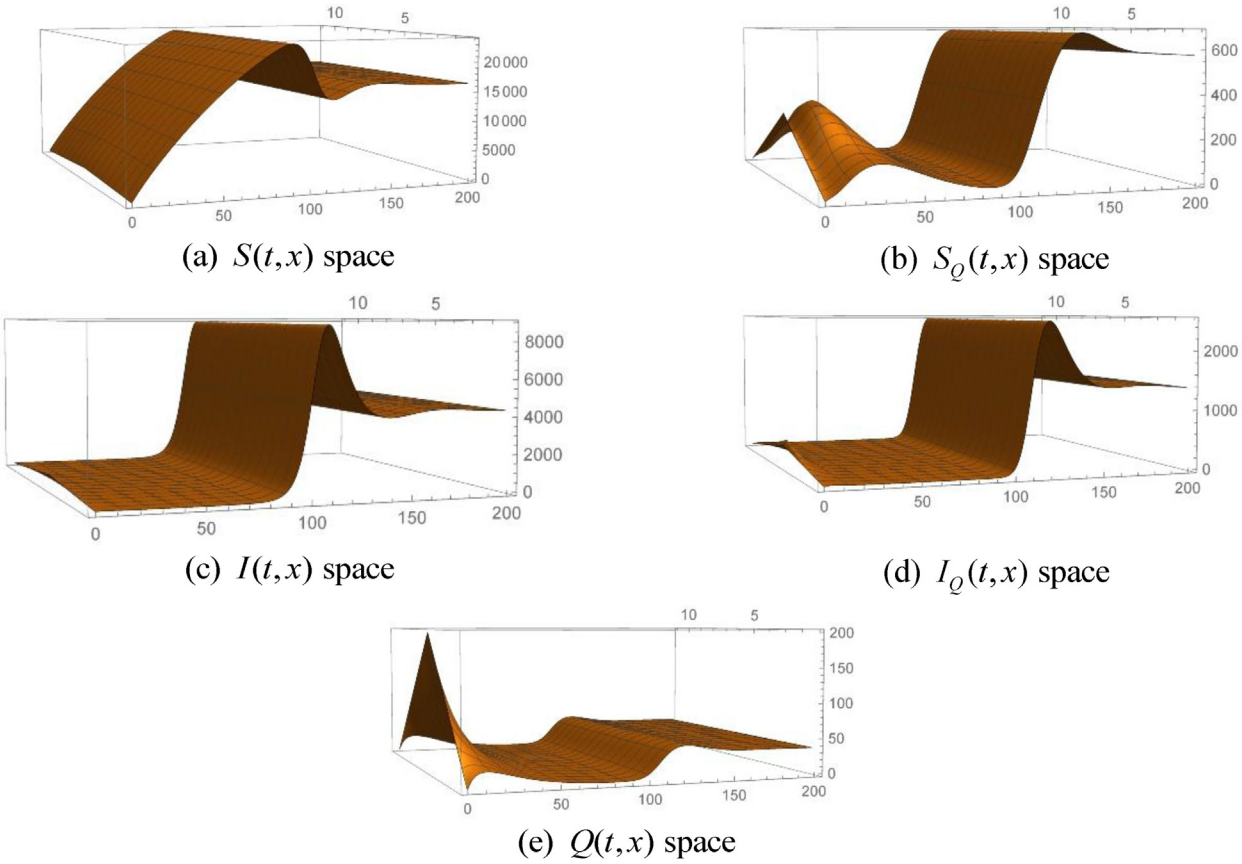

Fig. 13. Numerical simulation results for disease free equilibrium point.

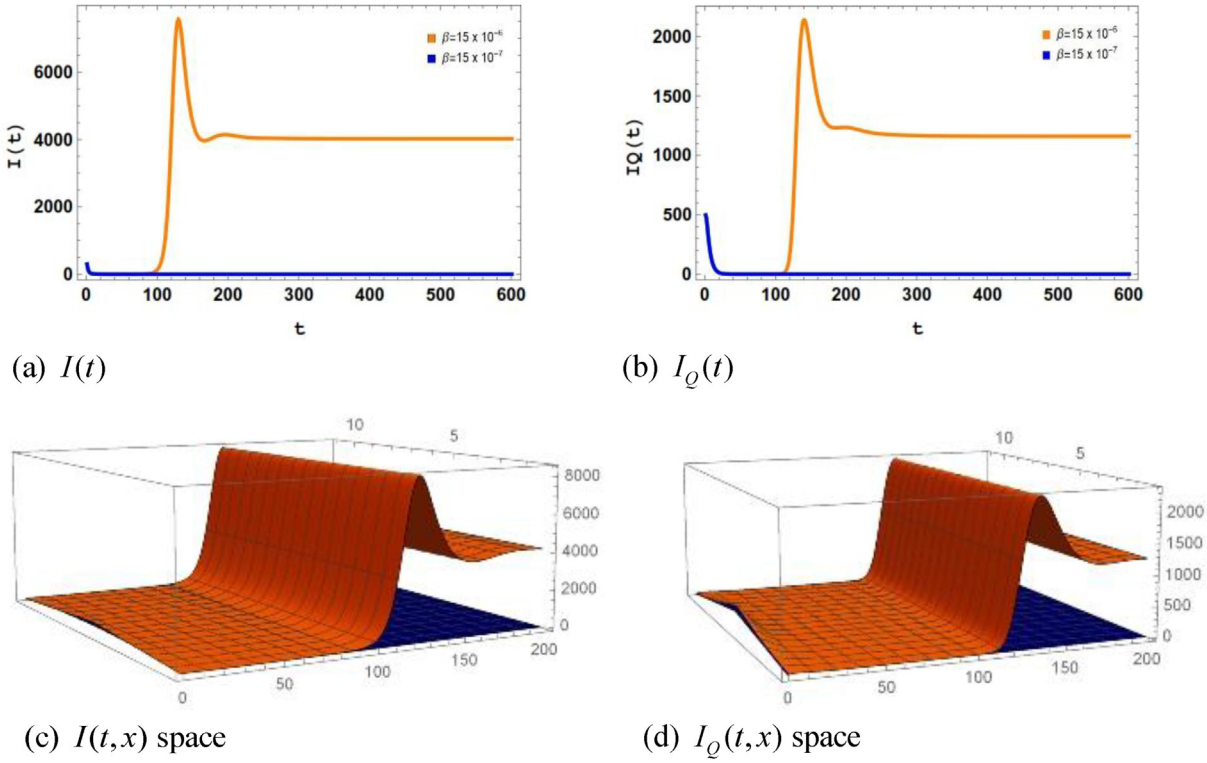

Fig. 14. Numerical simulation of I, I_Q with different values of $\beta = 15{*}10^{-6}$ and $15{*}10^{-7}$.

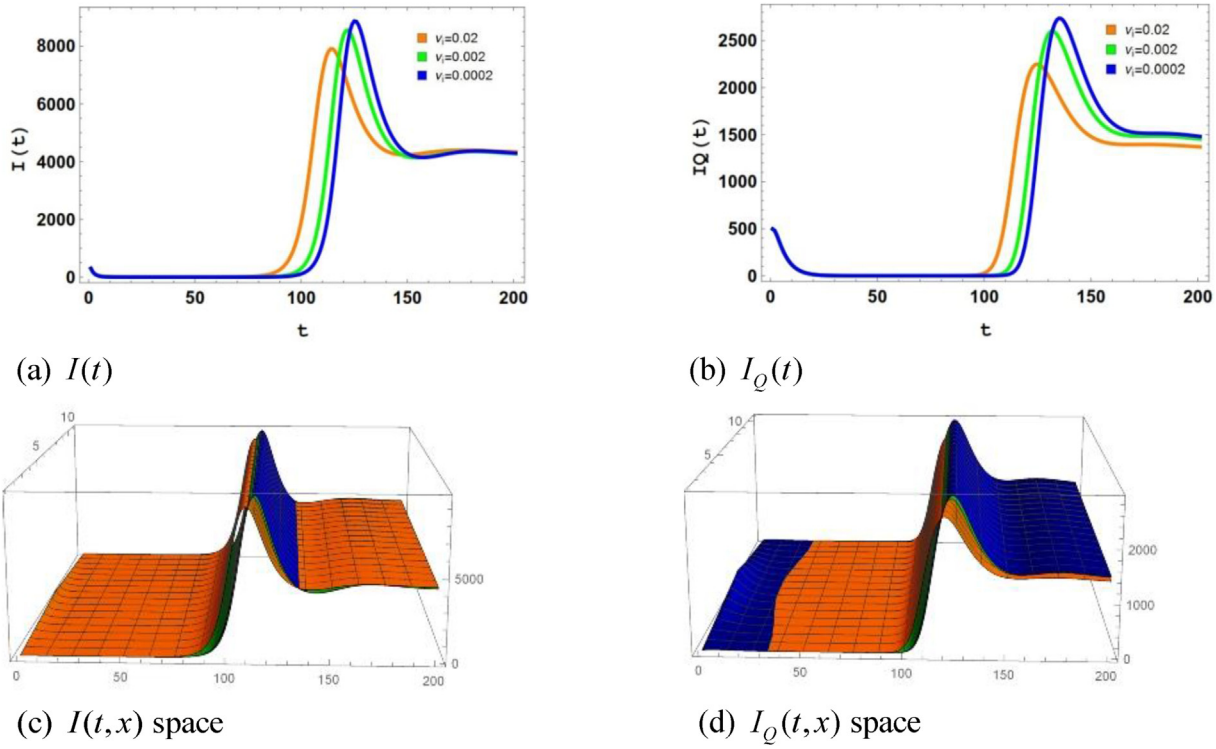

Fig. 15. Numerical simulation of I, IQ with different values of $\nu_i = 0.02, 0.002, 0.0002$.

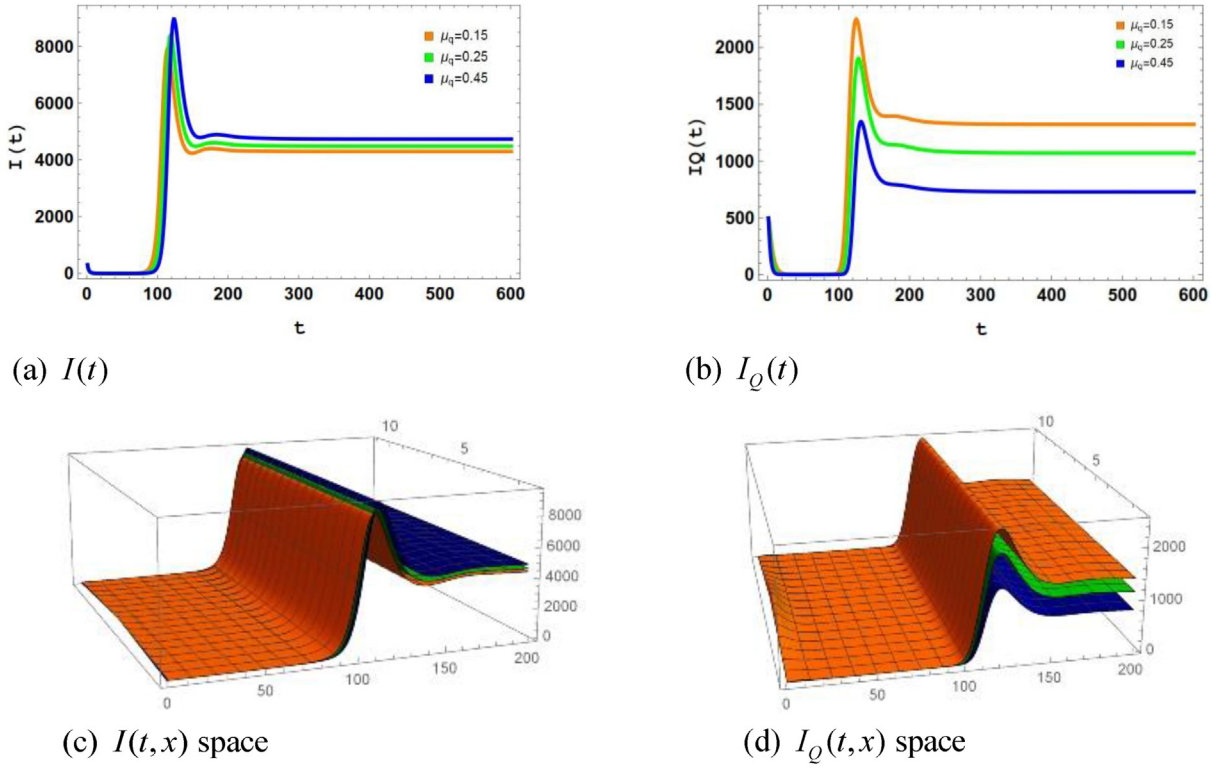

Fig. 16. Numerical simulation of I, IQ with different values of $\mu_q = 0.15, 0.25, 0.45$.

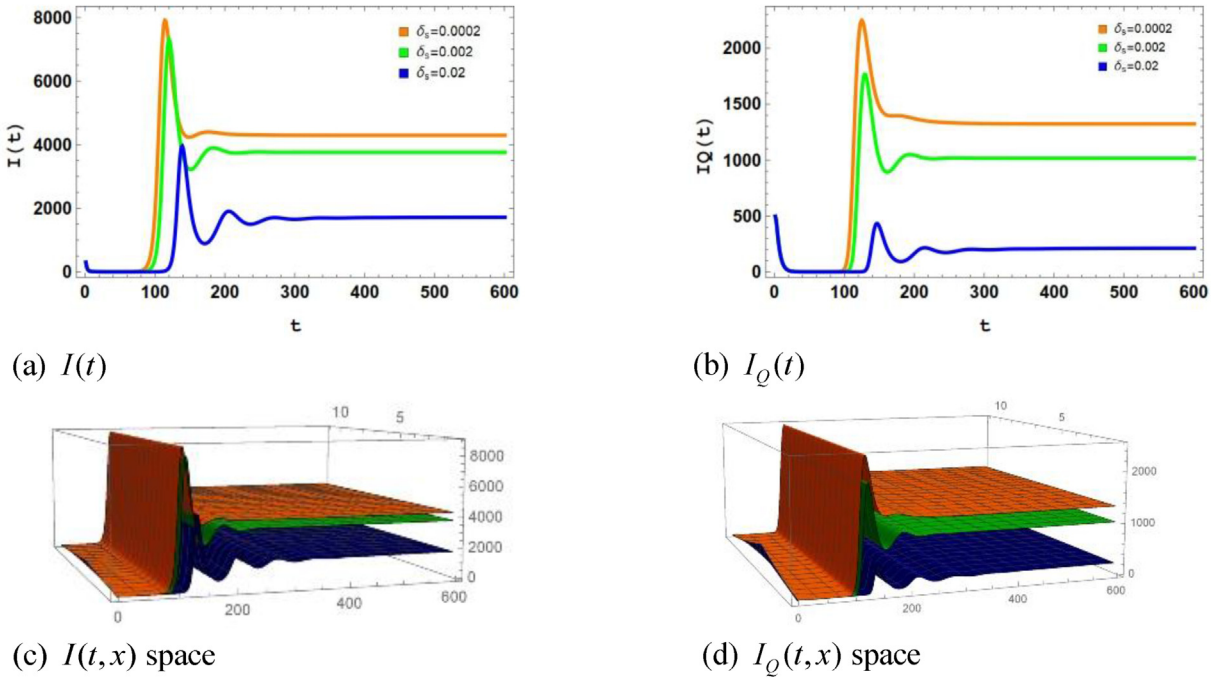

Fig. 17. Numerical simulation of I, IQ with different values of $\delta_s = 0.02, 0.002, 0.0002$.

percentage of infected people continues to increase as in Fig. 16a and c. In Fig. 17, we made a comparison of different values of δ_s and their impact on the spread of the epidemic, where δ_s represents the rate of imposing the lockdown on healthy people who are exposed to infection. We find that by increasing the percentage of isolation, the number of epidemic infections decreases significantly.

7. Conclusion

In this paper, a comprehensive numerical study of lockdown models for COVID-19 is presented, focusing on both temporal and spatio-temporal aspects. The reproduction number is discussed as a crucial indicator for estimating the spread of the virus. The analysis includes a sensitivity analysis to assess the significance of pandemic parameters. Moreover, the stability regions of the models are investigated, along with the Von Neumann stability and consistency of the numerical scheme applied to the spatio-temporal model. Numerical methods such as the CFD and RK-5 are employed to analyze the numerical results and facilitate comparison under various parameters. The findings provide valuable insights into the control and mitigation of COVID-19, contributing to our understanding of the disease dynamics and the effectiveness of different intervention strategies. The graphical numerical results of spatiotemporal results showed that all classes attain their maximum value in a specific region and then decrease when people go away from this area, which means that lockdown is an excellent control for decreasing infection. We discussed the effect of some parameters on controlling the spread of infection between individuals. Results showed that β and ν_i have a direct impact on the number of infections $I(t)$, so that $I(t)$ increase or decrease by increasing or decreasing of them, while μ_q have an inverse impact on $I(t)$ and a direct impact on $I_Q(t)$ and finally δ_s which have an inverse impact on both $I(t)$ and $I_Q(t)$, so an increase in δ_s leads to a decrease in $I(t)$ and $I_Q(t)$. This shows the importance of applying lockdown to reduce infection and control it. Overall, this study contributes to the existing body of knowledge by providing a mathematical formulation and numerical analysis of lockdown models for COVID-19. The results offer valuable guidance for policymakers and healthcare professionals in implementing effective measures to control the spread of the virus and mitigate its impact on public health and the economy. Further research and refinement of these models can continue to enhance our understanding of the complex dynamics of infectious diseases and inform evidence-based decision-making in pandemic situations.

Availability of data and materials

Data sharing is not applicable to this article as no datasets were generated or analyzed during the current study.

Authors' contributions

The authors declare that the study was realized in collaboration with equal responsibility. All authors read and approved the final manuscript.

Funding

No Funding.

Conflicts of interest

The authors declare that they have no competing interests.

Acknowledgements

All authors thank the editor chief of the journal, the editor who follows-up the paper, and all employees of the journal.

References

[1] Ali KK, Mona SM, Abdelrahman MI, Shaalan MA. Analytical and Numerical solutions for fourth order Lane-Emden-Fowler equation. Partial Differ Eqn Appl Math 2022;6:100430.
[2] Adem AR, Moretlo TS, Muatjetjeja B. A generalized dispersive water waves system: conservation laws; symmetry reduction; travelling wave solutions; symbolic computation. Partial Differ Eqn Appl Math 2022;7:100465.
[3] Karakoc SBG, Ali KK, Sucu DY. A new perspective for analytical and numerical soliton solutions of the Kaup−Kupershmidt and Ito equations. J Comput Appl Math 2023;421:114850.
[4] Ali KK, Karakoc SBG, Rezazadeh H. Optical soliton solutions of the fractional perturbed nonlinear schrodinger equation. TWMS J Applied and Engineering Mathematics 2020;10:930−9.
[5] Fatemeh A, Manmohan S, David R. Modelling of tumor cells regression in response to chemotherapeutic treatment. Appl Math Model 2017;48:96−112.
[6] Mondaini RP, Pardalos PM, editors. Mathematical modelling of biosystems, vol. 102. Springer Science & Business Media; 2008.
[7] Djaouea S, Kolayea GG, Abboubakar H, Ari AA, Damakoa I. Mathematical modeling analysis and numerical simulation of the COVID-19 transmission with mitigation of control strategies used in Cameroon. Chaos, Solit Fractals 2020;139: 1−15.
[8] Chayu Y, Jin W. A mathematical model for the novel coronavirus epidemic in Wuhan. China Math biosc and eng 2020; 17:2708−24.
[9] Koura AF, Raslan KR, Ali KK, Shaalan MA. Numerical analysis of a spatio-temporal bi modal coronavirus disease pandemic. Appl Math and Inf Sci 2022;16:729−37.
[10] Kucharski AJ, Russell TW, Diamond C, Liu Y, Edmunds J. Early dynamics of transmission and control of COVID-19: a mathematical modelling study. Inf Dise 2020;20:553−8.
[11] Baba SA, Yusuf A, Nisar KS, Abdel-Aty A, Nofal TA. Mathematical model to assess the imposition of lockdown during COVID-19 pandemic. Results Phys 2021;20:1−7.
[12] Valle JAM. Predicting the number of total COVID-19 cases and deaths in Brazil by the Gompertz model. Nonlinear Dynam 2020;102:2951−7.
[13] Mandal M, Jana S, Nandi SK, Khatua A, Adak S, Kar TK. A model based study on the dynamics of COVID-19, prediction and control. Chaos, Solit Fractals 2022;136:1−12.
[14] Biswas SK, Ghosh JK, Sarkar S, Ghosh U. COVID-19 pandemic in India: a mathematical model study. Non. Dyn 2020;102:537−53.
[15] Zhang Z, Zeb A, Egbelowo OF, Erturk VS. Dynamics of a fractional order mathematical model for COVID-19 epidemic. Adv Differ Equ 2020;420:1−16.
[16] Agarwal P, Ramadan MA, Rageh AAM, Hadhoud AR. A fractional-order mathematical model for analyzing the pandemic trend of COVID-19. Math Methods Appl Sci 2021; 45(8):4625−42.
[17] Wrapp D, Wang N, Corbett KS, Goldsmith JA, Hsieh C, Abiona O, et al. Cryo-EM structure of the 2019-nCoV spike in the prefusion conformation. Science 2020;367:1260−3.
[18] Rothe C, Schunk M, Sothmann P, Bretzel G, Froeschl G, Wallrauch C, et al. Transmission of 2019-nCoV infection from an asymptomatic contact in Germany. N Engl J Med 2020;382:970−1.
[19] Mohammadi H, Kumar S, Rezapour S, Etemad S. A theoretical study of the Caputo?Fabrizio fractional modeling for hearing loss due to Mumps virus with optimal control. J of Chaos, Solit & Fract 2021;144:110668.
[20] Tuan NH, Mohammadi H, Rezapour S. A mathematical model for COVID-19 transmission by using the Caputo fractional derivative. J of Chaos, Solit & Fract 2020;140: 110107.